Evaluating the performance of a space- and time-continuous deformation model

Corinna Harmening[1], Hans Neuner[1]

[1] Department of Geodesy and Geoinformation, TU Wien, Gußhausstraße 27-29, 1040 Vienna, Austria, (corinna.harmening@tuwien.ac.at, hans.neuner@tuwien.ac.at)

Key words: *B-spline surfaces; Correlation structure*; *Laser scanning*; *Least squares collocation*; *Locally stationary/homogeneous stochastic process; Space- and time-continuous deformation analysis; Step response*

ABSTRACT

The establishment of terrestrial laser scanning in engineering geodesy provides new possibilities, but also presents new challenges. An appropriate utilization of the huge amount of information contained in laser scanning point clouds requires the development of areal analyzing approaches. Currently, especially the development of a point cloud-based deformation analysis receives much attention.

In this contribution, a space- and time-continuous deformation model is introduced. The basis of this approach is formed by the initial object's geometry of the first measuring epoch, which is represented by a trend surface in terms of a best-fitting B-spline surface. The deviations of the point clouds measured in the subsequent epochs with respect to the trend surface reflect the deformations. These deviations are interpreted to be caused by a locally stationary and locally homogeneous stochastic process and, thus, they are modelled by means of stationary and homogeneous correlograms as well as slowly varying variances. The combination of the deterministic trend surface with this stochastic signal leads to an adjustment problem similar to a least squares collocation.

The focus of this contribution lies in the application of the deformation model to a deformed surface acting like a first-order system which follows the step response. Simulated data sets of five measuring epochs are used in order to analyze the approach's performance by investigating the filtering's residuals and by comparing the filtered data sets to nominal surfaces.

I. Introduction

The development of the laser scanner changed the analysis strategies of engineering geodetic problems from point-wise approaches to areal ones. Despite of the many advantages laser scanning provides, a variety of challenges occurs, especially when performing an areal deformation analysis (Holst and Kuhlmann 2016; Mukupa et al. 2016; Wunderlich et al. 2016). Missing point correspondences between two measuring epochs, the question concerning interpretable measures for areal deformations and the absence of appropriate error models for laser scanner measurements have to be mentioned in this context.

Areal analysis approaches meeting these challenges can be classified either to perform a point-to-point-based comparison (Little 2006), a point-to-surface-based comparison (Erdélyi et al. 2017) or a surface-to-surface-based comparison (Vezočnik et al. 2009) of the data sets describing the deformed object (Mukupa et al. 2016).

In this contribution an approach to an areal deformation analysis is introduced, allowing a point-to-surface based comparison with respect to a reference surface. Similar to a least squares collocation, the measured object is modelled to consist of three parts: A deterministic trend, describing the initial state of the object, a stochastic signal, representing the deformations, as well as the measuring noise accounting for the uncertainties caused by the measuring process. Due to the stochastic interpretation of the deformation and the respective modelling by means of locally stationary and locally homogeneous distance-depending covariograms, no identical points in different measuring epochs are required. Furthermore, a stable estimation of the stochastic relationships is possible, even if only few measuring epochs are available.

The introduced model is applicable even to very specific deformation types, e.g. the step response of a first-order system, and it provides satisfying results even in this "borderline" situation.

The paper is structured as follows: Section II provides the mathematical basics, which are needed for developing the presented approach. In section III the data sets, on which the approach is applied, are introduced. Furthermore, the relationship between a shifting of a B-spline surface's control point following a step response and the deformation of the respective surface is investigated. The space- and time-continuous analysis approach for deformation modelling is derived and applied to the simulated data sets in section IV. The results of the approach's application are presented and discussed in section V. Finally, in section VI a conclusion is drawn and an outlook is given.

II. Mathematical Basics

A. *Deformation processes*

The basic idea for the simulation of deformation processes is that an object behaves like a first-order system. Thus, its movement $y(t)$ caused by forces $x(t)$ acting on it can be described by means of a linear first-order differential equation

$$H_\infty x(t) = y(t) + T\dot{y}(t) \tag{1}$$

with H_∞, T: system specific constants (Pelzer 1976). The solution of this differential equation differs depending on the type of the acting forces. In this contribution, a closer look is taken at the sudden change of the acting forces (unit jump), as this synthetic signal is often used to identify the system's specific constants H_∞ and T.

Assuming a sudden change in load of $\Delta x = x_2 - x_1$ at a certain time t_0, the object reacts according to the step response and the resulting deformation can be described by (Pelzer 1976):

$$\Delta y(t) = H_\infty \left\{1 - e^{\left(-\frac{t-t_0}{T}\right)}\right\} \Delta x(t_0). \tag{2}$$

B. *B-spline surfaces*

A B-spline surface of degree *p* and *q* is defined by:

$$\widehat{\boldsymbol{S}}(u,v) = \sum_{i=0}^{n} \sum_{j=0}^{m} N_{i,p}(u)\, N_{j,q}(v) \boldsymbol{P}_{ij}\ . \tag{3}$$

A surface point $\widehat{\boldsymbol{S}}(u,v)$ is located by its surface parameters u and v on the surface and is computed as the weighted average of the $(n+1)$ x $(m+1)$ control points $\boldsymbol{P}_{ij}$ (Piegl and Tiller 1995). The respective weights are the functional values of the B-spline basis functions of degree p and q $N_{i,p}(u)$ and $N_{j,q}(v)$ which can be recursively computed by means of the Cox-de-Boor algorithm (Cox 1972; Boor 1972). The B-spline's domain is split into knot spans by two knot vectors $U = [u_0, \dots, u_r]$ and $V = [v_0, \dots, v_s]$ which are defined in direction of the surface parameters.

The division of the surface parameters' domain by means of the knot vectors leads to the property of locality, meaning that the shifting of one control point changes the surface only locally.

C. *Spatio-temporal stochastic processes*

A spatio-temporal stochastic process $Z(t, \boldsymbol{x})$ is defined to be stationary (homogeneous) if its statistical moments are constant over time t (location $\boldsymbol{x}$) and if its joint statistical moments depend only on the time lag τ (spatial distance d) between two observations (Schlittgen and Streitberg 2013; Cressie 2015). Temporal dependencies of stationary stochastic processes are usually modelled by means of covariance functions (Schlittgen and Streitberg 2013), whereas variograms (equation (4)) are used to model spatial dependencies (Cressie 2015):

$$\hat{\gamma}(\bar{d}_k) = \frac{1}{2|N_l|} \sum_{(\boldsymbol{x}_i, \boldsymbol{x}_j) \in N_l} \left(z(\boldsymbol{x}_i) - z(\boldsymbol{x}_j)\right)^2. \tag{4}$$

In equation (4) $z(\boldsymbol{x}_i)$ and $z(\boldsymbol{x}_j)$ are realizations of a stochastic process at a certain location $\boldsymbol{x}_i$ and $\boldsymbol{x}_j$ respectively. The variogram averages the squared differences over all $|N_l|$ point pairs whose distance $d_{ij} = ||\boldsymbol{x}_i - \boldsymbol{x}_j||$ is contained in the interval N_l $(l = 1, \dots, n_l)$ and, thus, is a function of the mean separation distance $\bar{d}_l$ of all point pairs belonging to interval N_l (Smith 2016).

When the process's variance σ^2 is known, a variogram can be transformed into a covariogram:

$$\hat{C}(\bar{d}_l) = \sigma^2 - \hat{\gamma}(\bar{d}_l). \tag{5}$$

Standardizing equation (5) with $\sigma^2 = \hat{C}(0)$ gives a correlogram:

$$\hat{\rho}(\bar{d}_l) = \frac{\hat{C}(\bar{d}_l)}{\hat{C}(0)}. \tag{6}$$

A stochastic process is defined to be locally stationary (homogeneous) if this correlogram can be split into the product of a stationary (homogeneous) correlogram and a slowly varying scale factor (Silverman 1957).

III. Data Sets

The data basis for the computations performed below are simulated data sets as they allow a comparison with nominal surfaces. Furthermore, the use of simulated data excludes an influence of a missing or an incorrect error model of the terrestrial laser scanner and the resulting pseudo-deformations.

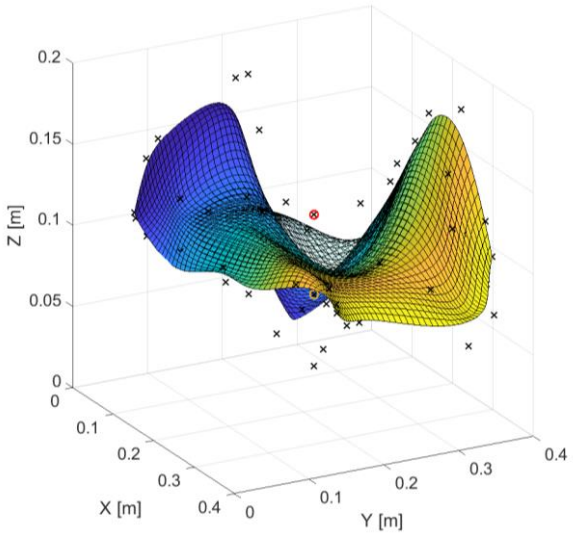

Figure 1. Deformed B-spline surface and its control points (black crosses). Solid surface: Non-distorted surface; opaque surface: Deformed surface for $t_5 = 120\ s$ resulting from an upwards shifting of the yellow encircled control point to the red marked position following a step response.

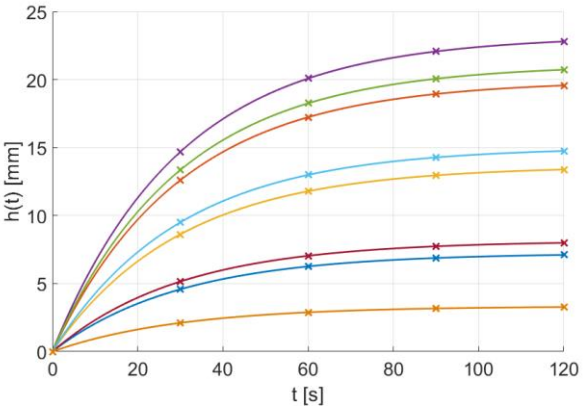

Figure 2. Temporal behaviour of a selection of surface points (crosses) which follow step responses (solid lines).

The non-distorted measuring object is represented by a B-spline surface with $n+1=9$ and $m+1=7$ control points and with dimensions of approximately 40 cm x 40 cm x 18 cm (solid surface in figure 1). This surface is deformed by moving the control point $\boldsymbol{P}_{4,5}$ (encircled in yellow in figure 1) according to equation (2) with $H_\infty = 1$ and $T = 30\ s$ upwards, resulting in the control point encircled in red.

As can be seen in figure 1 the shifting of one control point changes the surface only locally and leads to an uplift of the inner part of the surface. The surface is assumed to be acquired by means of a laser scanner during the deformation process at five equidistant points of time $t_1 = 0\ s, t_2 = 30\ s, \dots\ t_5 = 120\ s$.

However, as not the control point, but the surface itself has to be considered as the dynamic system following equation (2), firstly, it has to be verified that a step response of a control point leads to a step response of the B-spline surface itself.

For this reason, the five surfaces are sampled with a spatial resolution of approximately 6 mm. As the surface parameters u, v define point correspondences, the surface points' behavior over time can be analyzed.

In figure 2 the temporal behavior of eight exemplarily chosen surface points can be seen. As indicated by this point selection, the temporal behavior of all surface points can be expressed by means of equation (2) with a location dependent parameter Δx and with $H_\infty = 1$ and $T = 30\ s$ being equal in case of all eight curves. Thus, the surface itself can be regarded to be a dynamic system following the step response.

In a last step, measuring noise with a standard deviation of $\sigma_{\boldsymbol{\varepsilon}} = 1\ mm$ is added to the sampled surfaces, resulting in the data sets summarized in table 1.

Table 1. Simulated data sets

Abbr.	t [s]	Max. Deformation
$\mathbf{PC}^{(1)}$	0	0.0 cm
$\mathbf{PC}^{(2)}$	30	1.4 cm
$\mathbf{PC}^{(3)}$	60	1.9 cm
$\mathbf{PC}^{(4)}$	90	2.1 cm
$\mathbf{PC}^{(5)}$	120	2.2 cm

In accordance with equation (2), the maximum deformation increases rapidly from the first to the second measuring epoch, whereas it converges towards a constant value during the last three epochs.

IV. A Spatio-temporal Deformation Model

A. *Derivation of the spatio-temporal deformation model*

The deformation model is developed under the assumption that possible rigid body movements of the measuring object are detected and eliminated in advance, for example by using the B-spline-based approach introduced in (Harmening and Neuner 2016b). Thus, the measuring object considered in this contribution is solely affected by distortions. These distortions are assumed to be continuous so that the occurrence of discontinuities like edges and fractures is excluded.

The basic ideas of the developed deformation model are similar to those of a least squares collocation (LSC) (Moritz 1989). Thus, the observations $\boldsymbol{l}$ are modelled as the sum of the deterministic trend $\boldsymbol{Ax}$, which roughly approximates the observations, the stochastic signal $\boldsymbol{s}$, which carries information regarding the phenomenon in terms of stochastic relationships, as well as the measuring noise $\boldsymbol{\varepsilon}$, which models the uncertainty due to the measuring process:

$$E[\hat{\boldsymbol{l}}] = \boldsymbol{l} - \boldsymbol{\varepsilon} = \boldsymbol{A}\hat{\boldsymbol{x}} + \hat{\boldsymbol{s}}\,. \tag{7}$$

Both, signal and noise are assumed to be normally distributed with expectation $\mathbf{0}$ and covariance matrices $\boldsymbol{\Sigma}_{ss} = \sigma_0^2\,\boldsymbol{Q}_{ss}$ and $\boldsymbol{\Sigma}_{\varepsilon\varepsilon} = \sigma_0^2\,\boldsymbol{Q}_{\varepsilon\varepsilon}$ respectively. Furthermore, correlations between signal and noise are excluded (Heunecke et al. 2013).

In this approach, the trend is used to model the measuring object's initial and undistorted geometry, which is acquired during the first measuring epoch. Thus, the trend is the same throughout all epochs. The deformation is interpreted to be a spatio-temporal stochastic process and is solely modelled by means of the stochastic signal. Therefore, the trend is estimated once and is afterwards subtracted from the original observations. Combining this idea with the extension of equation (7) by κ epochs gives the functional model of the spatio-temporal deformation model:

$$\underbrace{\begin{bmatrix}\boldsymbol{l}^{(1)}\\ \boldsymbol{l}^{(2)}\\ \vdots\\ \boldsymbol{l}^{(\kappa)}\end{bmatrix}}_{\bar{\boldsymbol{l}}} - \underbrace{\begin{bmatrix}\boldsymbol{A}^{(1)}\\ \boldsymbol{A}^{(2)}\\ \vdots\\ \boldsymbol{A}^{(\kappa)}\end{bmatrix}}_{\bar{\boldsymbol{A}}} \boldsymbol{x}^{(1)} = \underbrace{\begin{bmatrix}\boldsymbol{s}^{(1)}\\ \boldsymbol{s}^{(2)}\\ \vdots\\ \boldsymbol{s}^{(\kappa)}\end{bmatrix}}_{\bar{\boldsymbol{s}}} + \underbrace{\begin{bmatrix}\boldsymbol{\varepsilon}^{(1)}\\ \boldsymbol{\varepsilon}^{(2)}\\ \vdots\\ \boldsymbol{\varepsilon}^{(\kappa)}\end{bmatrix}}_{\bar{\boldsymbol{\varepsilon}}}\,. \tag{8}$$

Due to the one-time estimation of the trend, the actual observations for the deformation analysis are the measurements' residuals with respect to the trend:

$$\bar{\boldsymbol{e}} = \bar{\boldsymbol{l}} - \bar{\boldsymbol{A}}\boldsymbol{x}^{(1)}\,. \tag{9}$$

By including a predicted signal $\bar{\boldsymbol{s}}'$, the compact form of the functional model results in

$$\bar{\boldsymbol{e}} = \underbrace{[\boldsymbol{I} \quad \boldsymbol{0} \quad \boldsymbol{I}]}_{\bar{\boldsymbol{B}}^T} \underbrace{\begin{bmatrix} \bar{\boldsymbol{s}} \\ \bar{\boldsymbol{s}}' \\ \bar{\boldsymbol{\varepsilon}} \end{bmatrix}}_{\bar{\boldsymbol{v}}} . \tag{10}$$

Equation (10) is a conditional model which is solved by

$$\begin{bmatrix} \hat{\bar{\boldsymbol{s}}} \\ \hat{\bar{\boldsymbol{s}}}' \\ \hat{\bar{\boldsymbol{\varepsilon}}} \end{bmatrix} = \begin{bmatrix} \boldsymbol{\Sigma}_{\bar{s}\bar{s}} \\ \boldsymbol{\Sigma}_{\bar{s}'\bar{s}} \\ \boldsymbol{\Sigma}_{\bar{\varepsilon}\bar{\varepsilon}} \end{bmatrix} \hat{\bar{\boldsymbol{k}}} \tag{11}$$

with

$$\hat{\bar{\boldsymbol{k}}} = (\boldsymbol{\Sigma}_{\bar{\varepsilon}\bar{\varepsilon}} + \boldsymbol{\Sigma}_{\bar{s}\bar{s}})^{-1} \bar{\boldsymbol{e}} \, . \tag{12}$$

As indicated by the formulas above, a modelling of the deformation following the proposed approach requires three steps (estimation of the trend, estimation of the signal and modelling of the noise) which will be discussed in detail in the following.

B. *Estimation of the trend*

The trend estimation is based on B-spline surfaces as they approximate even complex surfaces in a satisfying manner (Harmening and Neuner 2015).

When determining a best-fitting B-spline surface, usually only the location of the control points is estimated, resulting in a linear Gauß-Markov model. Methods for determining the remaining parameter groups can be found in (Bureick et al. 2016) (knot vectors), in (Harmening and Neuner 2015) (surface parameters) or in (Harmening and Neuner 2016a, 2017) (number of control points). In this study, nominal values known due to the simulation process are used for these remaining parameter groups.

Based on the ideas presented in the previous section, the point cloud of the first measuring epoch is used to estimate the B-spline surface's control points $\boldsymbol{P}^{(1)} = \boldsymbol{x}^{(1)}$:

$$\hat{\boldsymbol{P}}^{(1)} = (\boldsymbol{A}^{(1)^T} \boldsymbol{A}^{(1)})^{-1} \boldsymbol{A}^{(1)^T} \boldsymbol{l}^{(1)} . \tag{13}$$

The stochastic relationships between the observations caused by the measuring process are expressed by the identity matrix. Investigations regarding an improved modelling of the stochastic relationships between the observations can be found in (Kauker et al. 2017).

In equation (13) the observation vector $\boldsymbol{l}^{(1)}$ contains the observed coordinates in $x(u,v)$-, y(u,v)- and $z(u,v)$-direction and the design matrix $\boldsymbol{A}^{(1)}$ is filled by means of the B-spline basis functions $N_{i,p}(u)^{(i_\kappa)}$, $N_{j,q}(v)^{(i_\kappa)}$ in dependence of the surface parameters u, v, locating the observations on the surface to be estimated. Based on these control points, the trend can be estimated for each measuring epoch:

$$\hat{\boldsymbol{l}}^{(i_\kappa)} = \boldsymbol{A}^{(i_\kappa)} \hat{\boldsymbol{P}}^{(1)} \quad \text{with } i_\kappa = 1, \dots, \kappa. \tag{14}$$

The residuals of the trend estimation

$$\boldsymbol{e}^{(i_\kappa)} = \boldsymbol{l}^{(i_\kappa)} - \hat{\boldsymbol{l}}^{(i_\kappa)} \tag{15}$$

provide the basis for the modelling of the signal and can be exemplarily seen in figure 3 for the z-coordinate of data set **PC**$^{(5)}$.

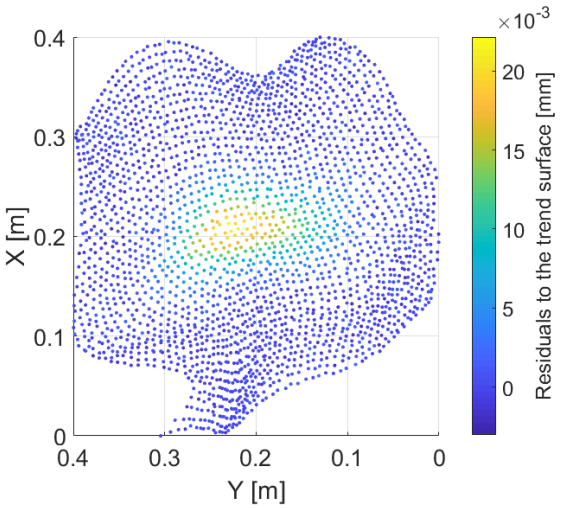

Figure 3. Residuals of the trend estimation in direction of the z-coordinate (data set **PC**$^{(5)}$)

C. *Estimation of the signal*

The first step of the signal modelling is the detection of the distorted regions as the non-distorted region of the measuring object is already completely described by means of the trend surface. In this study, a simple threshold consideration is used for this purpose: Each coordinate whose residual fulfils

$$\left| e_j^{(i_\kappa)} \right| > 1.5 \, \sigma^{(1)}, j = 1, \dots, n_l{}^{(i_\kappa)} \tag{16}$$

is allocated to the distorted region, with $\sigma^{(1)}$ being the estimated measuring noise of the first measuring epoch and $n_l{}^{(i_\kappa)}$ being the number of point observations in epoch (i_κ). As this simple threshold consideration results in a high probability of a type I error (points are erroneously marked to belong to the distorted region), a postprocessing step is performed which detects single points in non-distorted regions and relabels them.

Following the idea of the congruency model, the deformation process is interpreted to be mean-stationary and mean-homogeneous with the expectation of the signal being $E(\boldsymbol{s}) = 0$. Thus, the deformations are characterized by the process's variances and covariances. The former may strongly change over the distorted area as well as over the measuring period.

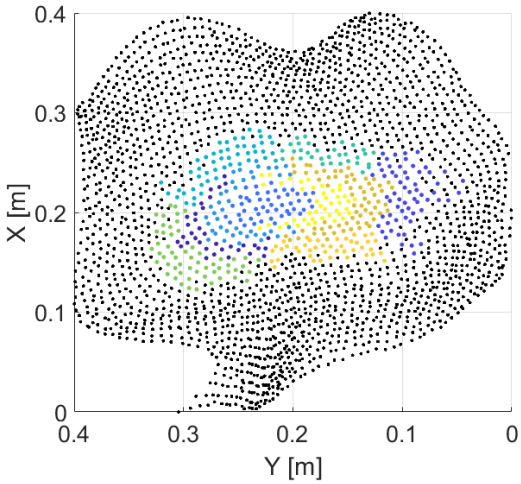

Figure 4. K-means-clustering of the residuals in direction of the z-coordinate (data set **PC**$^{(5)}$). Black: non-distorted region.

Consequently, the assumptions of strong stationarity and strong homogeneity are too restrictive. Thus, the principle of local stationarity is adopted in this context. The local variance as a slowly varying function of both, location and time, accounts for the changing magnitude of the residuals $\boldsymbol{e}^{(i_\kappa)}$, whereas the stationary and homogeneous correlation structure allows an estimation of the required quantities based solely on one realization of the stochastic process.

In order to account for the spatial variability of the variance, a clustering of $\boldsymbol{e}^{(i_\kappa)}$ is performed by means of a k-means clustering (Lloyd 1982) (cf. figure 4).

Assuming a common variance representative for each cluster, the respective standard deviations and, consequently, the variances are estimated by:

$$\sigma_j^{(i_\kappa)} = \frac{1}{3}\max(|\boldsymbol{e}_j^{(i_\kappa)}|) \tag{17}$$

with: $\boldsymbol{e}_j^{(i_\kappa)} \in c_j$,
$j = 1, \dots, n_c$ indicating the cluster
$i_\kappa = 2, \dots, \kappa$ indicating the epoch.

Afterwards, these values are used to normalize the residuals according to

$$\tilde{\boldsymbol{e}}_j^{(i_\kappa)} = \frac{\boldsymbol{e}_j^{(i_\kappa)}}{\sigma_j^{(i_\kappa)}}. \tag{18}$$

These normalized residuals provide the basis for the computation of empirical correlograms according to equations (4) - (6). Both, the modelling of the correlations within one measuring epoch and the modelling of the correlations between two measuring epochs is based solely on the spatial distance between the respective observations. The distinction between the spatial and the temporal correlations is solely realized by the estimation of different correlograms.

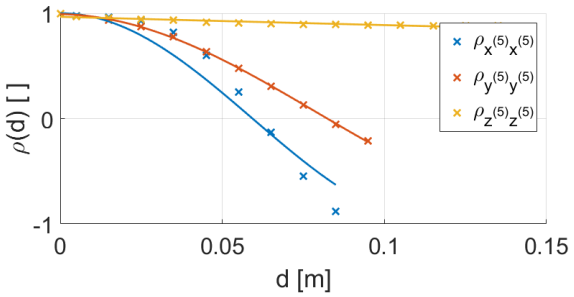

Figure 5. Empirical (crosses) and analytical correlograms (solid lines) within data set **PC**$^{(5)}$.

On the one hand, this procedure results in stable estimates even if only few measuring epochs are available. On the other hand, this procedure does not require identical points in different measuring epochs.

When having estimated the empirical correlations (crosses in figure 5), they are approximated by means of analytical positive definite functions, resulting in analytical correlograms (solid lines in figure 5). It has to be noted that the empirical correlograms reflect the superimposition of two stochastic processes: the white noise-process representing the measuring noise as well as the signal (correlated process) representing the deformation. The estimation of analytical correlograms directly separates them: The ratio between empirical correlation $\hat{\rho}(0)$ and analytical correlation $\rho(0)$ can be used to split the overall variance of each cluster into the variance of the noise and the variance of the signal (Smith 2016):

$$\frac{\hat{\rho}(0)}{\rho(0)} = \frac{\sigma_{\boldsymbol{s}}^2 + \sigma_{\boldsymbol{\varepsilon}}^2}{\sigma_{\boldsymbol{s}}^2}. \tag{19}$$

The analytical functions provide the basis for setting up the correlation matrix $\boldsymbol{R}_{\bar{s}\bar{s}}$, consisting of $\kappa \, x \, \kappa$ submatrices:

$$\boldsymbol{R}_{\bar{s}\bar{s}} = \begin{bmatrix} \boldsymbol{R}_{\boldsymbol{ss}}^{(1)(1)} & \cdots & \boldsymbol{R}_{\boldsymbol{ss}}^{(1)(\kappa)} \\ \vdots & \ddots & \vdots \\ \boldsymbol{R}_{\boldsymbol{ss}}^{(\kappa)(1)} & \cdots & \boldsymbol{R}_{\boldsymbol{ss}}^{(\kappa)(\kappa)} \end{bmatrix}. \tag{20}$$

In equation (20) the submatrices on the main diagonal model the correlations within one measuring epoch, whereas the matrices on the minor diagonals reflect the correlations between two epochs.

Each of the submatrices is built up coordinate-wise and contains the analytical correlations as a function of the distance between the respective points.

In a last step, this correlation matrix is converted into the variance-covariance matrix of the signal $\boldsymbol{\Sigma}_{\bar{s}\bar{s}}$ by taking into account the locally stationary and locally homogeneous variances computed by equation (17).

D. *Modelling of the noise*

In this study, the noise is simulated to be non-correlating so that the variance-covariance matrix of the noise $\boldsymbol{\Sigma}_{\bar{\varepsilon}\bar{\varepsilon}}$ is a diagonal matrix. Although the assumption

of non-correlating noise does not hold for measured data sets, this simplifying assumption has to be seen as a first step towards an areal deformation analysis. Consequently, no separation of the two types of correlations (due to the measuring process and due to the deformation process) is necessary in this study. As the two variance were already separated during the determination of the analytical correlograms, $\boldsymbol{\Sigma}_{\bar{\varepsilon}\bar{\varepsilon}}$ can be directly set up.

V. Filtering Results

Having determined the trend surface as well as $\boldsymbol{\Sigma}_{\bar{s}\bar{s}}$ and $\boldsymbol{\Sigma}_{\bar{\varepsilon}\bar{\varepsilon}}$, the formulas derived in section IV can be used to filter the simulated point clouds.

In a first step, the filtering's residuals are analysed. The residuals' spatial distribution in direction of the z-coordinate can be seen in figure 6 for point cloud **PC**(5). As can be seen, the residuals' magnitude varies almost randomly over the surface with the residuals of the distorted area being slightly smaller than those of the non-distorted area. The transition zone between those two areas is recognizable due to the accumulation of relatively large residuals (light yellow), indicating that an improved method for distinguishing between distorted and non-distorted regions may improve the results. Nevertheless, with few exceptions, the residuals' magnitude lies within the range defined by the threefold standard deviation of the measuring noise.

Table 2 presents the filtering's residuals of all measuring epochs by means of statistical parameters describing the residuals' distribution. As can be seen, the residuals' distribution of the first epoch closely follows the normal distribution, which was used to generate the measuring noise. Thus, the pure trend estimation separates the measuring noise in a satisfying way.

For the remaining measuring epochs, the distributions of the residuals in direction of the z-coordinate differ slightly more from the normal distribution of the simulated measuring noise: The standard deviations are smaller, whereas the kurtosis lies within the range of [3.4,…,3.7], indicating slightly leptocurtic distributions.

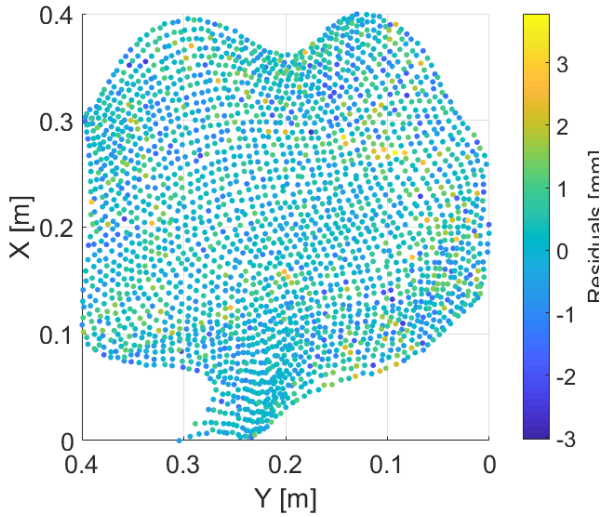

Figure 6. Residuals of the filtering in direction of the z-coordinate (data set **PC**(5))

Table 2. Statistical parameters of the filtering's residuals

	PC(1)	**PC**(2)	**PC**(3)	**PC**(4)	**PC**(5)
mean($\hat{\boldsymbol{\varepsilon}}_x$) [mm]	3e-13	-0.02	-3e-3	0.01	3e-4
mean($\hat{\boldsymbol{\varepsilon}}_y$) [mm]	4e-13	0.02	6e-3	5e-3	0.02
mean($\hat{\boldsymbol{\varepsilon}}_z$) [mm]	8e-14	0.10	0.09	0.09	0.10
std($\hat{\boldsymbol{\varepsilon}}_x$) [mm]	0.98	0.58	0.48	0.45	0.45
std($\hat{\boldsymbol{\varepsilon}}_y$) [mm]	0.98	0.49	0.67	0.49	1.15
std($\hat{\boldsymbol{\varepsilon}}_z$) [mm]	0.98	0.82	0.87	0.85	0.80
skewness($\hat{\boldsymbol{\varepsilon}}_x$) []	0.08	0.06	-0.04	-0.25	-0.10
skewness($\hat{\boldsymbol{\varepsilon}}_y$) []	0.02	-0.09	-0.90	-0.20	0.40
skewness($\hat{\boldsymbol{\varepsilon}}_z$) []	0.01	0.04	0.06	0.11	0.17
kurtosis($\hat{\boldsymbol{\varepsilon}}_x$) []	3.1	9.1	8.2	6.1	6.4
kurtosis($\hat{\boldsymbol{\varepsilon}}_y$) []	3.0	6.9	27.9	8.2	37.8
kurtosis($\hat{\boldsymbol{\varepsilon}}_z$) []	2.9	3.5	3.6	3.4	3.7

Due to the superimposition of trend, signal and noise in these measuring epochs, a filtering of the noise proves to be more challenging than in the first measuring epoch, where only the trend has to be subtracted. Nevertheless, as the deviations are minimally and as there does not exist a relationship between the deformation's magnitude and the filtering's quality, the results are promising.

In contrast, the statistical parameters in direction of x- and y-coordinate reveal a severe deviation to the measuring noise's distribution. On the one hand, this behavior is caused by the definition of the coordinate system (cf. figure 1). As the direction of the deformation corresponds to the direction of the z-coordinate, whereas the measuring object's two principal components lie within the x/y-plane, the data sets are very insensitive for determining deformations in these directions. On the other hand, this behavior is caused by the coordinate-wise treatment of the observations during the analysis process.

Due to the use of simulated data sets, a comparison of the filtered data with respect to nominal surfaces is possible. In figure 7 the spatial distribution of the filtered residuals with respect to the nominal surface can be seen.

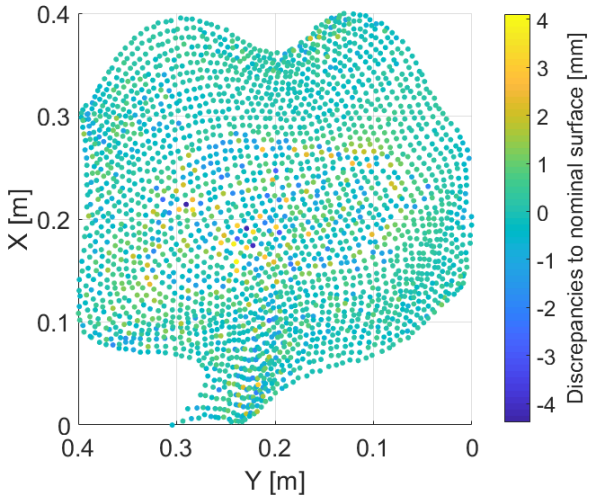

Figure 7. Discrepancies to the nominal surface in direction of the z-coordinate (data set **PC**(5))

Table 3. Properties of the discrepancies between the filtered point cloud and the nominal surfaces

	PC(1)	**PC**(2)	**PC**(3)	**PC**(4)	**PC**(5)
mean(d_x)[mm]	-0.01	-0.01	-0.03	0.01	-0.01
mean(d_y)[mm]	-0.03	0.02	0.02	0.01	0.03
mean(d_z)[mm]	0.02	0.11	0.08	0.08	0.08
max(d_x)[mm]	1.07	4.37	2.97	3.47	4.32
max(d_y)[mm]	0.49	3.24	4.68	3.41	4.77
max(d_z)[mm]	1.08	4.33	4.24	3.50	4.11
min(d_x)[mm]	-0.76	-4.01	-3.26	-4.72	-4.42
min(d_y)[mm]	-2.02	-4.15	-3.96	-3.29	-5.65
min(d_z)[mm]	-0.87	-3.17	-3.45	-2.72	-4.39
skewness(d_x)[]	0.27	0.01	-0.10	-0.07	-0.08
skewness(d_y)[]	-0.90	-0.05	0.19	0.01	-0.08
skewness(d_z)[]	-0.42	0.49	0.05	0.25	0.22
kurtosis(d_x) []	6.9	3.8	3.2	3.4	3.6
kurtosis(d_y) []	11.4	3.5	3.6	3.3	4.5
kurtosis(d_z) []	5.6	6.0	5.4	4.7	7.2

The discrepancies' magnitudes allow a distinction between the distorted area and the non-distorted one, as the pure trend estimation increases the observations' precision due to the measuring process and leads to discrepancies of $\pm 1\ mm$ in the non-distorted region. The discrepancies' magnitude is larger in the distorted region but lies – with few exceptions – within the threefold standard deviation of the measuring noise. These exceptions either lie within the transition zone between distorted and non-distorted area or in that area where the largest deformation occurs. Despite of these systematics, the discrepancies' magnitudes vary randomly within both areas, indicating a compensation of the systematics caused by the deformation process as well as maintaining of the measuring process' precision in the distorted area due to the stochastic model.

Table 3 summarizes the properties of the discrepancies between the filtered point cloud and the nominal surfaces for all five measuring epochs.

The averaged discrepancies being close to zero for all measuring epochs as well as the small values of the skewness indicate an unbiased filtering with respect to the nominal surface. Minimal and maximal values of the discrepancies are slightly smaller for the z-coordinate than for x- and y-coordinate, supporting the conclusions provided by table 2 regarding the insensitivity with respect to deformations in these two coordinate directions. Although the minimal and maximal discrepancies are larger than the threefold standard deviation of the noise, the large values for the kurtosis in direction of the z-coordinate reveal an accumulation of the discrepancies around zero and support the model's approximation quality.

VI. Conclusions

A. *Summary*

In this contribution, an approach for an areal deformation analysis was introduced and applied to simulated data sets.

The deformation model is based on a B-spline surface representing the undistorted object acquired in the first measuring epoch as well as on a locally stationary and locally homogeneous signal describing the deformation process. The description of the deformation process requires the distinction between distorted and non-distorted areas of the measuring object, the determination of local variances as well as the estimation of a homogeneous and stationary correlation structure.

The application to simulated data sets representing a surface deforming according to the step response of a first-order system reveals promising results: Even in case of relatively large deformations compared to the measuring object's size, the deformation can be described with an accuracy in the order of the measuring noise.

B. *Outlook*

Although the majority of systematics caused by the deformation are eliminated by means of the stochastic modelling, the results reveal that a simple threshold consideration in order to distinguish between distorted and non-distorted areas of the object has weaknesses. Thus, further investigations with regard to the classification of the distorted regions are necessary.

The application of the deformation model was restricted to simulated data sets following the step response in this contribution. In future, the range of investigated deformation processes will be extended by applying the model to other types of typical deformation processes (linear deformations, periodic deformations etc.).

Another restriction was made by assuming non-correlated measuring noise. The use of a more realistic noise behavior when simulating the data and the respective investigations regarding the separability of correlated noise and correlated signal is the first step towards the application to measured data sets instead of simulated ones.

As already indicated in the development of the approach, a prediction of the signal is possible. As this allows a prediction of the deformation within one measuring epoch as well as into non-measured epochs, a space- and time-continuous description of the deformed measuring object is possible.

VII. Acknowledgements

This article presents the results developed during the research project "Integrierte raumzeitliche Modellierung unter Nutzung korrelierter Messgrößen zur Ableitung von Aufnahmekonfigurationen und Beschreibung von Deformationsvorgängen" (IMKAD) (1706–

N29), which is funded by the Austrian Science Fund (FWF).

References

Boor, C. de (1972). On calculating with B-splines. In: *Journal of Approximation Theory,* Vol. 6, No. 1, pp. 50–62.

Bureick, J., Alkhatib, H., Neumann, I. (2016). Robust Spatial Approximation of Laser Scanner Point Clouds by Means of Free-form Curve Approaches in Deformation Analysis. In: *Journal of Applied Geodesy*, Vol. 10, No. 1, pp. 27-35.

Cox, M. G. (1972). The Numerical Evaluation of B -Splines. In: *IMA Journal of Applied Mathematics*, Vol. 10, No. 2, pp. 134–149.

Cressie, N. A. C. (2015). Statistics for spatial data. Revised edition. New York: John Wiley & Sons (Wiley classics library).

Erdélyi, J., Kopáčik, A., Lipták, I., Kyrinovič, P. (2017). Automation of point cloud processing to increase the deformation monitoring accuracy. In: *Applied Geomatics,* Vol. 9, No. 2, pp. 105–113.

Harmening, C., Neuner, H. (2015). A constraint-based parameterization technique for B-spline surfaces. In: *Journal of Applied Geodesy,* Vol. 9, No. 3, pp. 143-161.

Harmening, C., Neuner, H. (2016a). Choosing the Optimal Number of B-spline Control Points (Part 1: Methodology and Approximation of Curves). In: *Journal of Applied Geodesy,* Vol. 10, No. 3, pp. 139-157.

Harmening, C., Neuner, H. (2016b). Detecting rigid body movements from TLS-based areal deformation measurements. In: *Proceedings of the 78th FIG Working Week 2016*.

Harmening, C., Neuner, H. (2017). Choosing the optimal number of B-spline control points (Part 2: Approximation of surfaces and applications). In: *Journal of Applied Geodesy,* Vol. 11, No. 1, pp. 43-52.

Heunecke, O., Kuhlmann, H., Welsch, W., Eichhorn, A., Neuner, H. (2013). Handbuch Ingenieurgeodäsie. 2nd revised and extended edition. Berlin: Wichmann.

Holst, C., Kuhlmann, H. (2016). Challenges and Present Fields of Action at Laser Scanner Based Deformation Analyses. In: *Journal of Applied Geodesy,* Vol. 10, No. 1, pp. 17-25.

Kauker, S., Harmening, C., Neuner, H., Schwieger, V. (2017). Modellierung und Auswirkung von Korrelationen bei der Schätzung von Deformationsparametern beim terrestrischen Laserscanning. In: *Ingenieurvermessung 17, ed. by W. Lienhart*, pp. 321–336.

Little, M. (2006). Slope Monitoring Strategy at PPRust Open Pit Operation. In: *Proceedings of the International Symposium on Stability of Rock Slopes in Open Pit Mining and Civil Engineering*.

Lloyd, S. (1982): Least squares quantization in PCM. In: *IEEE Transactions on Information Theory,* Vol. 28, No. 2, pp. 129–137.

Moritz, H. (1989): Advanced physical geodesy. 2nd ed. Karlsruhe: Wichmann.

Mukupa, W.; Roberts, G. W.; Hancock, C. M.; Al-Manasir, K. (2016). A review of the use of terrestrial laser scanning application for change detection and deformation monitoring of structures. In: *Survey Review,* Vol. 36, No. 5, pp. 1–18.

Pelzer, H. (1976): Zur Analyse von permanent registrierten Deformationen. In: *Internationaler Kurs für Ingenieurvermessungen hoher Präzision, Technische Hochschule Darmstadt*, pp. 781–796.

Piegl, L., Tiller, W. (1995). The NURBS Book. Berlin, Heidelberg: Springer Berlin Heidelberg (Monographs in Visual Communications).

Schlittgen, R., Streitberg, B. H. J. (2013). Zeitreihenanalyse. 9th ed. München: Oldenbourg (Lehr- und Handbücher der Statistik).

Silverman, R. (1957). Locally stationary random processes. In: *IEEE Transactions on Information Theory,* Vol. 3, No. 3, pp. 182–187.

Smith, T. E. (2016). Notebook on Spatial Data Analysis (http://www.seas.upenn.edu/ ese502/ #notebook). Available online at [online] http://www.seas.upenn.edu/ ese502/#notebook.

Vezočnik, R., Ambrožič, T., Sterle, O., Bilban, G., Pfeifer, N., Stopar, B. (2009). Use of terrestrial laser scanning technology for long term high precision deformation monitoring. In: *Sensors (Basel, Switzerland),* Vol. 9, No. 12, pp. 9873–9895.

Wunderlich, T., Niemeier, W., Wujanz, D., Holst, C., Neitzel, F., Kuhlmann, H. (2016). Areal deformation analysis from TLS point clouds - the challenge. In *Allgemein Vermessungsnachrichten (avn),* Vol. 123, No. 11-12, pp. 340–351.